Prepared for submission to JINST

20TH International Symposium on Laser-Aided Plasma Diagnostics
10–14/9/2023
Kyoto (Japan)

Tangentially viewing phase contrast imaging for turbulence measurements in toroidal fusion devices

S. Coda

Ecole Polytechnique Fédérale de Lausanne (EPFL), Swiss Plasma Center (SPC), CH-1015 Lausanne, Switzerland

E-mail: stefano.coda@epfl.ch

Abstract: Phase contrast imaging (PCI) is an established and powerful technique for measuring density fluctuations in plasmas and has been successfully applied to several fusion devices. Rooted in a concept first developed for microscopy, PCI belongs to the category of internal-reference interferometers and has been shown to possess superior qualities among such techniques, particularly in terms of spatial linearity. In essence, it produces a true image of fluctuations in the plane perpendicular to the propagation direction of the probing laser beam, provided their characteristic spatial scale is smaller than the beam width. The measurement in itself is line-integrated and thus not spatially resolved longitudinally to the beam. However, the properties of the turbulence itself can be exploited to achieve longitudinal resolution, particularly when the beam propagates nearly tangentially to the magnetic field. This assertion has been recently rigorously tested through numerical modeling, which has revealed significant additional complexity while confirming the general principle. Tangential PCI has been employed extensively in the TCV tokamak and has resulted in a rich body of work on broadband microturbulence in the ion-temperature-gradient/trapped-electron-mode range and on geodesic acoustic modes. A similar diagnostic arrangement is also at an advanced planning stage for the new superconducting tokamak JT-60SA.

Keywords: Plasma diagnostics - interferometry, spectroscopy and imaging

Contents

1 Introduction

In a nuclear-fusion reactor, the fusion power must exceed the power supplied to the plasma, which, in steady-state conditions, must balance the power lost through radiation and energy transport. Consequently, one of the basic goals of tokamak research has been the containment of such losses to their minimum irreducible values. The inescapable rate of energy transport caused by Coulomb collisions is known in toroidal geometry as *neoclassical transport*. In general, transport is found to be well in excess of this rate. This excess *anomalous transport* is widely attributed, with increasing experimental backing, to microturbulence, i.e., microinstabilities that develop into a nonlinear, turbulent state.

A complete understanding of turbulence remains elusive even in the case of incompressible fluids, described by the Navier-Stokes equation. In a plasma, the addition of electromagnetic forces between charged particles to the pressure-gradient and viscous forces clearly complicates the problem even further. New degrees of freedom are introduced by the collective plasma motion: the nonlinear interaction between eddies in fluids is then augmented by the interaction between the fundamental plasma oscillation modes, and between these and the eddies. In spite of this complexity, increasingly sophisticated high-fidelity models, such as those that are applied in gyrokinetic codes, are nevertheless shedding more light on the nature of this turbulent behavior.

Detailed measurements of the fluctuating components of various plasma quantities are also necessary, and the connection between microinstabilities and transport has been a strong motivation for the development of diagnostics to measure fluctuations in tokamaks. Advances in diagnostic techniques are constantly occurring. Fluctuation imaging is a relative newcomer to experimental plasma physics but is rapidly gaining acceptance and constantly finding new applications, particularly for structures at the edge of fusion plasmas [1, 2] but also in the core as an extension of traditional techniques such as reflectometry [3] and electron-cyclotron emission [4]. Just as flow visualization is revolutionizing the field of experimental fluid dynamics, so are imaging techniques responding to the need for increased sophistication in the study of thermonuclear plasmas. The conditions encountered in modern-day tokamaks are especially conducive to the utilization of imaging diagnostics. The gradient scale lengths of the macroscopic plasma parameters in a tokamak, particularly at the edge, are often of the same order as the fluctuation wavelengths – close in turn

to the ion gyroradius, typically a few cm – effectively blurring the distinction between average and fluctuating quantities. A similar situation is encountered to some extent in the time domain, with very fast large-scale transients, such as the L–H transition and Edge Localized Modes (ELMs), occurring over magnetohydrodynamic time scales (typically less than 0.1 ms) comparable to the period of the fluctuations. A direct spatial mapping with good temporal resolution is clearly the most natural representation of such a plasma.

This contribution focuses on developments in the phase-contrast imaging technique. This was an invention [5] with long-lasting impact in the field of microscopy, with wide-ranging applications to biology and medicine. It was applied to plasmas for the first time to study gas jets and high-density plasma shock waves in air and argon [6]. Since then, applications to plasmas have been almost exclusively in the context of high-temperature plasmas and nuclear-fusion research. While the technique can be described as well-established and mature at this point, it is still not widespread. The first use of PCI in fusion devices was on the TCA tokamak [7], after which applications to several other devices followed: DIII–D [8], CDX–U [9], Alcator C–Mod [10], TEXT–U [11], LHD [12], TCV [13], Wendelstein 7–X [14], HL–2A [15], KT–5C [16].

In practical implementations on fusion devices, the probing light beam is a Gaussian-shaped laser beam, most typically a CO_2 laser of 10.6 μm wavelength. A particular focus of this paper is the achievement of spatial localization with this technique, when used in conjunction with tangential launching of the associated light beam - i.e., providing the beam direction vector with a large toroidal component.

The remainder of this paper is organized as follows: section 2 will describe the principles of the phase-contrast technique and compare its properties with other, related techniques; section 3 will discuss the basis for localizing the measurement and the practical implementation of the associated method, using in particular the PCI diagnostic installed on the TCV tokamak as a concrete example. Brief conclusions are offered in section 4.

2 The phase-contrast imaging technique

We consider a light wave of wave number $\mathbf{k_0}$ and angular frequency ω_0 propagating through a plasma and encountering, and being scattered by, a monochromatic density perturbation of wave number $\mathbf{k}$ and angular frequency ω. We restrict our analysis to the *coherent*, or *collective* scattering limit, in which the perturbation's wavelength $2\pi/k$ is much longer than the Debye length. We also confine our remarks to the limit $k/k_0 \ll 1$. Under these conditions, it is well known that the scattered power is peaked about the scattering angles ϕ_B given by the Bragg relation [17]

$$\phi_B = \pm\frac{k}{k_0}. \tag{2.1}$$

The wave-wave coupling rules impose constraints both on the scattering directions *and* on the direction of propagation of the scattering perturbation. No scattering occurs at angles other than the Bragg angles, and no scattering occurs if the density wave is not nearly perpendicular to the electromagnetic wave (Fig. 1(a)). Also, the two Bragg angles $\pm k/k_0$ correspond to two different density waves, propagating in the different, albeit very close, directions specified by Eq. (2.1) and shown in Fig. 1(b). Thus a single sinusoidal density perturbation generates at most *one* scattered

wave. These conditions are, however, simplified and idealized. In reality the interaction volume, and specifically the interaction length along z, L_z, is not infinite; as a result, k_z, the longitudinal component of the density fluctuation wave vector, can only be defined to within an uncertainty π/L_z, and the selection rules for the density waves are relaxed to a finite angular spread, $\delta\theta \approx \delta k_z/k$. If there is substantial overlap between the positive and negative scattering cones, both scattered waves exist simultaneously. This condition can be written as

$$L_z < \frac{\pi k_0}{k^2}. \tag{2.2}$$

The regime in which this condition is satisfied is known as the *Raman-Nath regime* [18]. The opposite limit, in which only one scattering angle is allowed, is called the *Bragg regime*. It can be shown that the Raman-Nath regime, combined with near-field detection, coincides with the region of validity of geometrical optics [19].

In the geometrical-optics approximation, the interaction of the light wave with the plasma, seen now simply as a refractive medium, is characterized by a phase shift

$$\Delta\Phi = k_0 \int \mathcal{N} dz, \tag{2.3}$$

where $\mathcal{N}$ is the index of refraction. For $\omega_0 \gg \omega_p$ (ω_p being the plasma frequency) the amplitude is essentially unchanged, and Eq. (2.3) reduces to

$$\Delta\Phi = \lambda_0 r_e \int n_e dz, \tag{2.4}$$

where $\Delta\Phi$ is in radians, n_e is the electron density, $\lambda_0 = 2\pi/k_0$, and $r_e \equiv e^2/(m_e c^2)$ is the classical radius of the electron.

Under the conditions considered thus far, therefore, measuring density fluctuations requires measuring the phase change they induce on the probing light wave. This phase change due to fluctuations can be assumed to be much smaller than unity. The effect they have on the electric field of the wave can then be written as

$$\mathbf{E}_s(\mathbf{y}, t) = \mathbf{E}_0(\mathbf{y}, t) e^{i\tilde{\varphi}(y,t)} \simeq \mathbf{E}_0(1 + i\tilde{\varphi}), \tag{2.5}$$

where E_0 and E_s are the unperturbed and scattered fields, respectively, $\tilde{\varphi}$ is the fluctuating phase shift, and y indicates a coordinate perpendicular to the direction of propagation z of the light wave.

If the scattered and unscattered components of the wave could somehow be separated, and a $\pm 90°$ phase shift could be applied to the unscattered component alone, the resulting field could be written

$$\mathbf{E}'_s = \mathbf{E}_0(\pm i + i\tilde{\varphi}). \tag{2.6}$$

Now to first order in $\tilde{\varphi}$ the intensity can be written

$$|E'_s|^2 = |E_0|^2 (1 \pm 2\tilde{\varphi}). \tag{2.7}$$

This operation therefore results in an intensity with a fluctuating component that is *directly proportional* to the phase of the original beam. Thus on the image plane a square-law detector

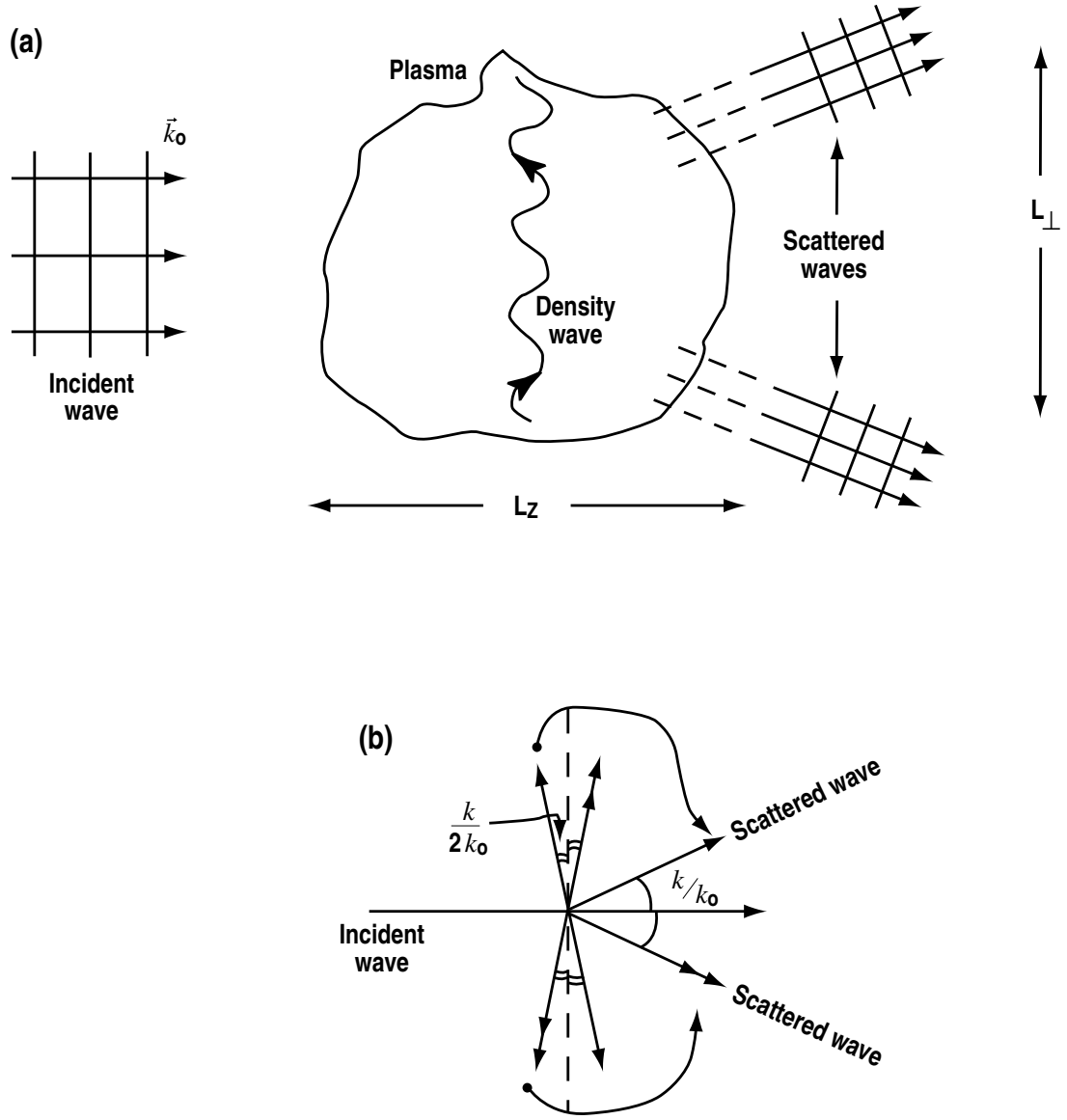

Figure 1: (a) Interaction of an electromagnetic wave with a plasma; (b) selection rules for scattering vectors and scattered waves.

would register a signal proportional to the line integral of the density. Note that this would be true even if the phase shift were not exactly 90°, although the proportionality factor is maximum in that case.

This is the foundational principle of the phase-contrast technique [19, 20]. The different directions of propagation of the unscattered and scattered components permit them to be easily separated in the focal plane of a collecting optic (see Fig. 2). According to the laws of geometrical optics, a ray impinging on a lens of focal length F at a small angle θ to the optical axis reaches the focal plane at a distance $y = F\theta$ from the optical axis. This implies that the unscattered rays are focused at the center of the focal plane, while the scattered rays intercept the same plane at varying

distances from the center, depending on the wave number of the perturbation that generated them.

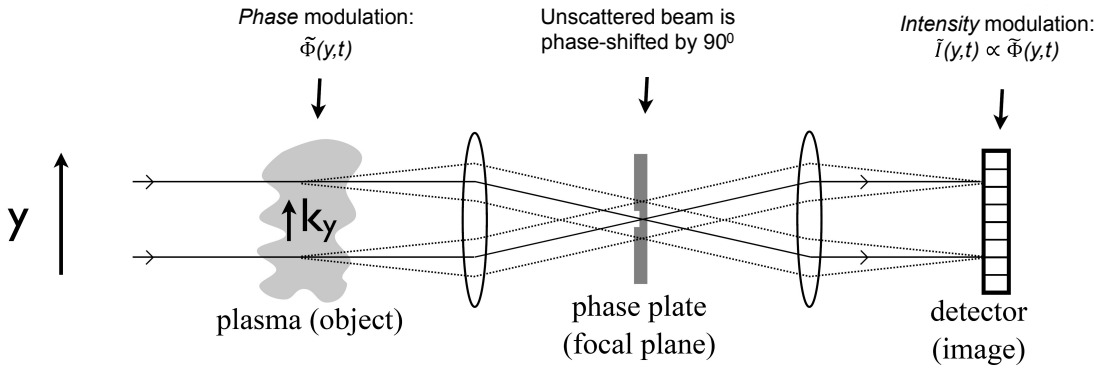

Figure 2: Schematics of phase-contrast technique.

Having thus separated the two components, the necessary phase shift can be introduced by means of a thin refractive strip (for a one-dimensional bundle) or dot (in the two-dimensional case) located at the center of the focal plane and designed to increase the path length by a quarter of a wavelength. This region is called the *conjugate area*, whereas the remainder of the focal plane is known as the *complementary area*. The same effect can be achieved by a reflecting component with a suitable area depressed by one-eighth of a wavelength. The conjugate area must be comparable to the size of the focal spot to achieve reasonable results.

A strong attenuation of the unscattered signal, which acts in practice as a local oscillator in an internal-interference scheme, can be applied to permit an increase in the achievable signal-to-noise ratio, provided sufficient light power is available. In practice, a sensitivity approaching 1 μrad/$\sqrt{\text{MHz}}$ can be achieved.

We can now step back and ask whether this truly is a desirable way to measure phase variations in a light wave. An obvious competitor is interferometry. Both interferometry and phase-contrast imaging can be combined with an imaging arrangement. Interferometry provides the optimal response function: it will measure the phase precisely, irrespective of the wavelength of the perturbation, and produce a perfect image of the phase perturbation. Interferometry relies, however, on an external phase reference. Combining two light beams that travel along different paths makes the result vulnerable to mechanical vibrations. In the phase-contrast method, on the other hand, the reference and probing beams in effect travel together and encounter all the same optics, and any vibration-induced shifts therefore cancel out. This technique is thus far more sensitive and is optimal for the detection of small fluctuations. The price to pay is that *absolute* phase shifts cannot be detected, since there is no absolute reference; only phase *variations* across the light beam can be measured. A different way to state this is that the response function of the phase-contrast technique must vanish for $k = 0$ (k being, once again, the wave number of the density perturbation): in practice, the cutoff wavelength is approximately equal to the width of the beam.

Let us now then assume that an internal-reference technique, which must be based on some form of beam manipulation, i.e., spatial filtering, is chosen for sensitivity purposes. Is phase contrast the best option? Considering a rather general spatial filter as shown in Fig. 3, which includes three separate focal-plane zones with different transmission coefficients and phase shifts, it

has been proven that the phase-contrast case is the only one that provides true phase imaging in the relevant wave-number range: i.e., it transforms the phase information into a measurable amplitude *point by point*, whereas all other sets of parameters results in a convolution [19]. To express this differently, phase contrast alone yields a linear response in wave-number space, with no phase shift, except at wave numbers below the cutoff value. Phase contrast also provides the largest absolute signal, maximizing the signal-to-noise ratio. The response function in the space of fluctuation wave numbers in standard conditions, such as those encountered on the TCV tokamak, is shown in Fig. 4.

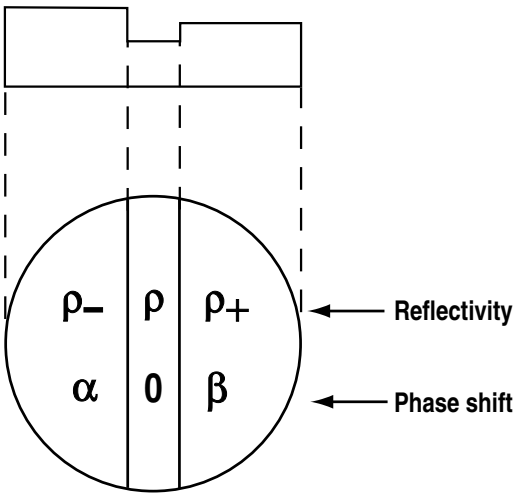

Figure 3: General reflective spatial filter.

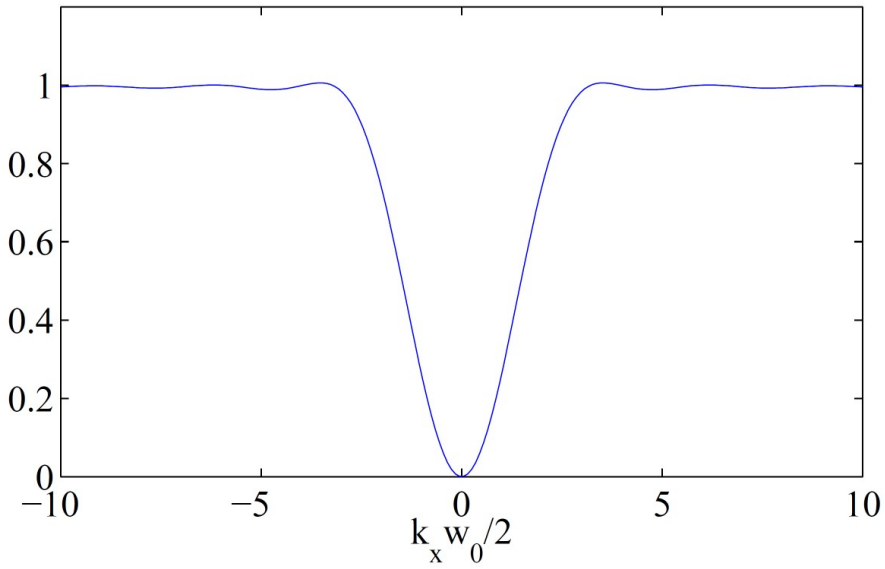

Figure 4: Modulus of the response function of phase-contrast imaging in wave-number space.

3 Localized phase-contrast imaging measurements

The PCI technique described in the previous section provides nearly unlimited spatial resolution across the width of the beam, but performs a line integration along the beam. It is not, in its basic form, a localized measurement. However, it has long been recognized that selection rules apply to these scenarios in the wave-number domain. In particular, the symmetry of fluctuations along the field lines [21] can also be exploited in conjunction with spatial filtering to achieve spatial localization along the direction of propagation. This technique is based on the existence of two separate selection rules for the detectable wave vectors of density fluctuations: the symmetry along the magnetic-field lines implies that the wave vector must be perpendicular to the field, and the scattering selection rule forces the vector to be perpendicular to the direction of propagation of the beam, lest the line integration cancel out the perturbation in question. Therefore, the measured fluctuation wave vector at each point along the beam must be perpendicular to the plane defined by the beam axis and by the local magnetic field. The combined effects of toroidal geometry and magnetic shear cause the direction of the wave vector to be different at different points along the beam [22]. Spatial filtering can then be used to select a direction, thus localizing the measurement to the region in which that particular direction satisfies the selection rules (see Fig. 5).

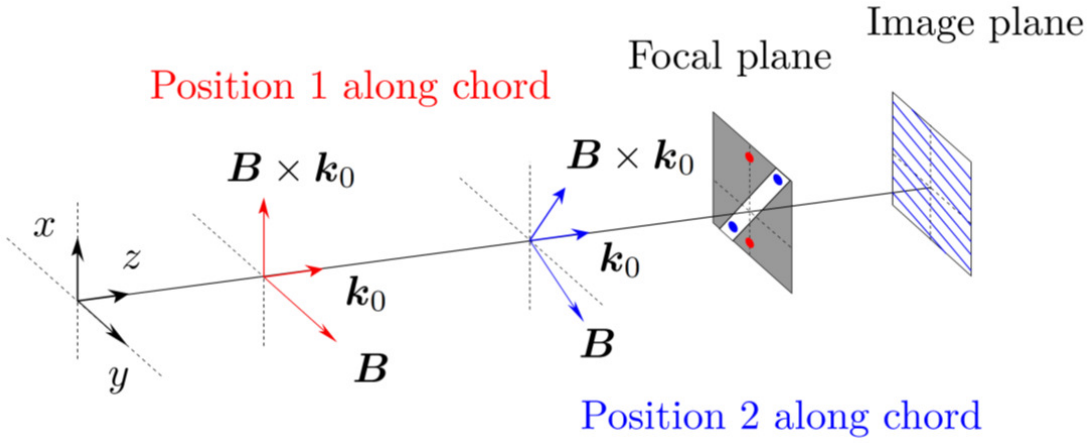

Figure 5: Illustration of the rotation, along the beam path, of the fluctuation wave vector contributing to the signal, and the corresponding mechanism for selecting the direction of the wave vector and thus the measurement location.

For this technique to be effective in providing localized measurements, the selected fluctuation wave-vector direction must rotate rapidly as a function of a linear coordinate along the light beam. This occurs most prominently in a tokamak in the case of a probing beam with a large toroidal component, i.e. a *tangential* launching (reflecting the fact that the beam will be near-tangent to the magnetic field at some point along its path).

The ability to select a wave-vector angle is limited by diffraction in practice, related to the finite width of the light beam. The half-width of a Gaussian spot in wave-number space, defined as the $1/e^2$ point of the intensity, is given by $\Delta k = 2/w_0$, where w_0 is the half-width of the Gaussian beam. Thus the resolution in the selection of the angle of the wave-vector with respect to a reference

direction is

$$\Delta\theta = \pm \arctan\left(\frac{2}{kw_0}\right). \tag{3.1}$$

As the angular selectivity thus increases with k, the achievable localization will also improve with increasing k. In most cases of interest very good localization can be achieved, particularly at the tangency point, as illustrated by Fig. 6 for TCV, for the beam geometry shown in Fig. 7. At the tangency point, in addition, the derivative of the radial flux-surface coordinate ρ with respect to the linear coordinate along the beam vanishes. As seen in Fig. 6(b), this magnifies the localization effect when expressed in terms of the ρ coordinate.

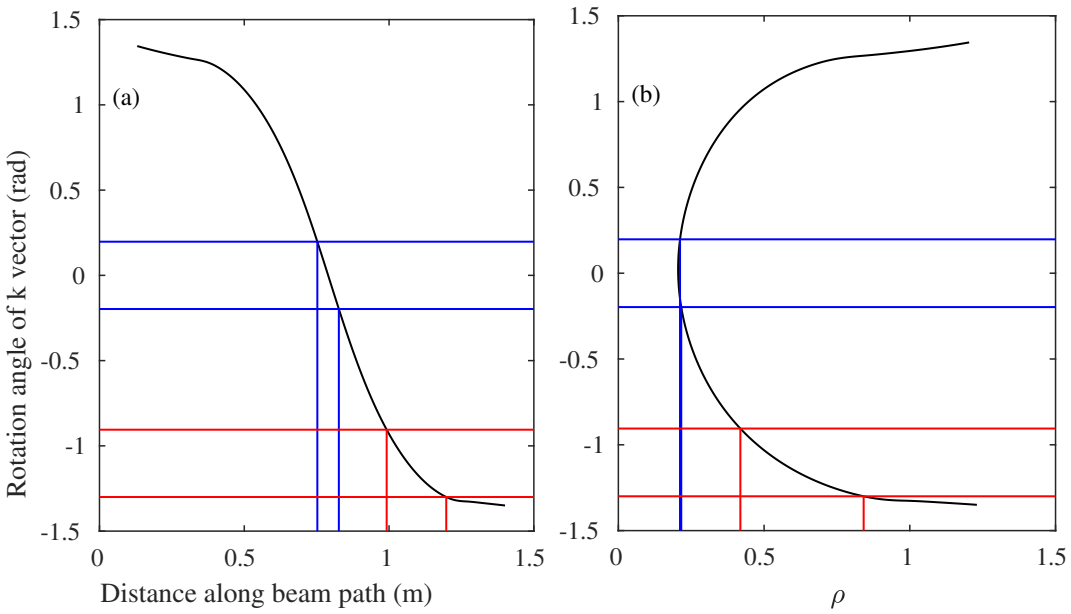

Figure 6: (a) Rotation angle of **k** vector of density fluctuations in the plane perpendicular to the beam propagation direction (cf Fig. 5), vs linear distance along the beam path, for a standard TCV shot and $k = 4$ cm^{-1}; the two horizontal bands illustrate the diffraction-limited angular resolution, and are projected onto vertical bands illustrating the spatial localization at two different locations. (b) The same but now as a function of the radial flux-surface coordinate (ρ).

Two types of spatial filters have been employed to implement the wave-vector selection: filters characterized by a straight slit and filters featuring a wedge-shaped opening (Fig. 8) [22]. In the former case, the width of the slit corresponds to the width of the Gaussian spot, providing optimum resolution at all values of the fluctuation wave number k. The reasoning behind the wedge-shaped filter is to endow all values of k with the same spatial resolution as the lowest value that can be resolved by the PCI technique, i.e., $k_c \simeq 3/w_0$. In this way one sacrifices resolution at high k for the sake of maintaining a linear response and creating a true spatial image of fluctuations over the same volume.

It should be noted, however, that this spatial selection principle is predicated on the assumption that fluctuations possessing a finite wave-vector component parallel to the direction of propagation of the beam would be averaged out and vanish entirely in the final signal. This cannot be an exact assumption, as residual signal will always remain in a finite system. Numerical calculations in

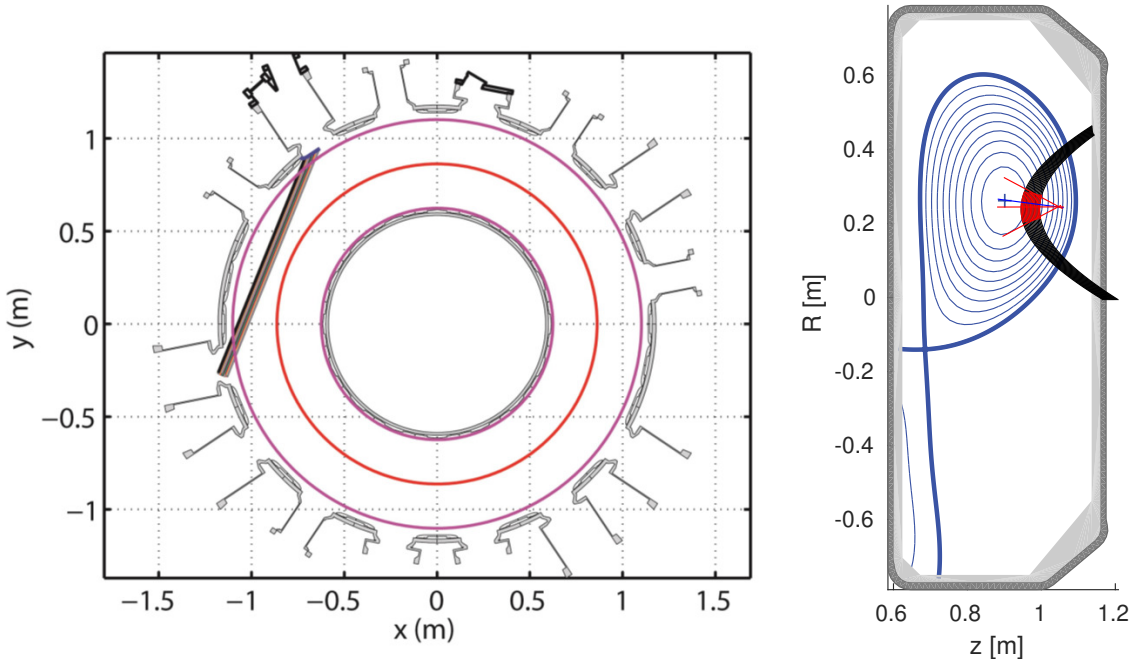

Figure 7: (Left) Top view and (right) poloidal projection of the PCI beam path on TCV.

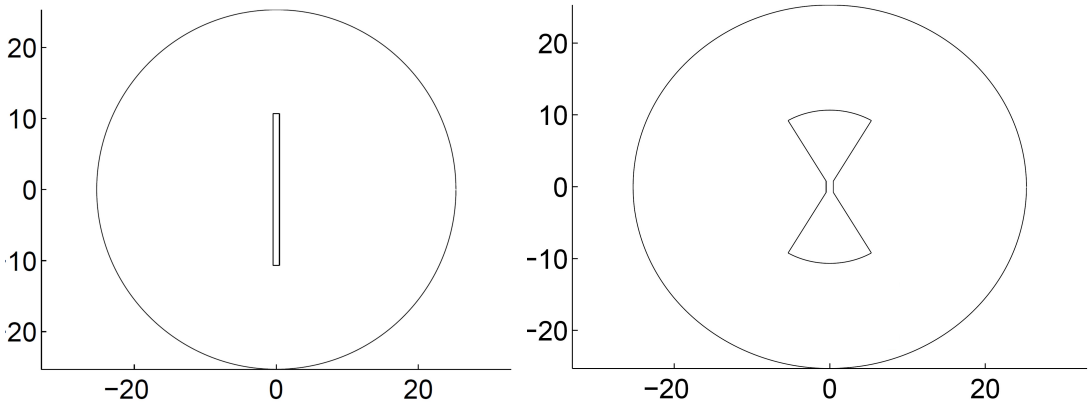

Figure 8: Two types of spatial filters used to select the direction of the measured wave vector: (left) straight slit; (right) wedge-shaped opening.

realistic geometries are required to test the assumption. This can be done by using the formalism of a *synthetic PCI diagnostic*, which has been developed to permit meaningful comparisons of results from high-fidelity gyrokinetic simulations with experiment. By using this formalism, it has been shown that using the straight-slit type of filter permits indeed achieving resolutions that are as good as or better than those estimated using the simple considerations discussed above [23]. However, this is not generally true of the wedge-shaped filter, and it is therefore concluded that the hope to achieve a more faithful image representation by using such a filter is probably misplaced.

The TCV PCI diagnostic has been employed for well over a decade and has produced a wealth of data, in particular on core turbulence in the ion-temperature-gradient/trapped-electron-mode

microinstability regimes and on geodesic acoustic modes [24–26]. Up to now the system has been able to access wave numbers up to 13 cm^{-1} with a bandwidth of under 1 MHz. However, an upgrade is now underway to extend this to 60 cm^{-1} and 10 MHz, respectively, with also much increased spatial resolution. This will open the possibility for the first time to access electron-temperature-gradient modes.

A tangential PCI diagnostic is also in an advanced stage of development for the JT–60SA tokamak, where it is expected to provide important new data on turbulence in more reactor-relevant regimes. The geometry planned for JT–60SA will yield the best spatial resolution near the plasma boundary and near the magnetic axis; the resolution elsewhere will however also be adequate for investigating the spatial profile of core turbulence [27].

4 Conclusions

Phase-contrast imaging is a powerful and mature laser-based technique for studying fluctuations, turbulent or otherwise, in magnetic-confinement fusion devices. It has superior properties in terms of sensitivity and linearity, providing a direct spatial representation of plasma density fluctuations. When endowed with a tangential launching geometry in a toroidal device, it can be augmented with a spatial filtering technique that removes the constraint of chord integration and provides good spatial localization, especially near the point of tangency of the laser beam with the flux surfaces. Tangential PCI has been demonstrated extensively on the TCV tokamak and is planned to be employed in the new JT–60SA device.

References

[1] S.R. Haskey, N. Thapar, B.D. Blackwell, J. Howard, *Rev. Sci. Instrum.* **85** (2014) 033505.

[2] S.J. Zweben, J.L. Terry, D.P. Stotler, R.J. Maqueda, *Rev. Sci. Instrum.* **88** (2017) 041101.

[3] Y. Wang, B. Tobias, Y.-T. Chang, J.-H. Yu, M. Li, F. Hu, M. Chen, M. Mamidanna, T. Phan, A.-V. Pham, J. Gu, X. Liu, Y. Zhu, C.W. Domier, L. Shia, E. Valeoa, G.J. Kramer, D. Kuwahara, Y. Nagayama, A. Mase, N.C. Luhmann Jr., *Nucl. Fusion* **57** (2017) 072007.

[4] L. Yu, C.W. Domier, X. Kong, S. Che, B. Tobias, H. Park, C.X. Yu, N.. Luhmann Jr, *J. Instrum.* **7** (2012) C02055.

[5] F. Zernike, *Physica* **1** (1934) 689.

[6] H.M. Presby and D. Finkelstein, *Rev. Sci. Instrum.* **38** (1967) 1563.

[7] H. Weisen, *Plasma Phys. Contr. Fusion* **28** (1986) 1147.

[8] S. Coda, M. Porkolab, T.N. Carlstrom, *Rev. Sci. Instrum.* **63,** 4974 (1992).

[9] E. Lo, J. Wright, R. Nazikian, *Rev. Sci. Instrum.* **66** (1995) 1180.

[10] A. Mazurenko, M. Porkolab, D. Mossessian, J.A. Snipes, X.Q. Xu, W.M. Nevins, *Phys. Rev. Letters* **89** (2002) 225004.

[11] R. Chatterjee, G.A. Hallock, and M.L. Gartman, *Rev. Sci. Instrum.* **66** (1995) 457.

[12] K. Tanaka, C.A. Michael, L.N. Vyacheslavov, A.L. Sanin, K. Kawahata, T. Akiyama, T. Tokuzawa, S. Okajima, *Rev. Sci. Instrum.* **79** (2008) 10E702.

[13] C.A. de Meijere, S. Coda, Z. Huang, L. Vermare, T. Vernay, V. Vuille, S. Brunner, J. Dominski, P. Hennequin, A. Kr amer-Flecken, G. Merlo, L. Porte, L. Villard, *Plasma Phys. Contr. Fusion* **56** (2014) 072001.

[14] Z. Huang, E. Edlund, M. Porkolab, J-P. B ahner, L.-G. B ottger, C. v. Sehren, A. von Stechow, O. Grulke, *J. Instrum.* **7** (2012) C02055.

[15] S.B. Gong, Y. Yu, M. Xu, A.P. Sun, T. Lan, H. Liu, W.L. Zhong, Z.B. Shi , H.J. Wang, Y.F. Wu, B.D. Yuan, S.F. Mao, M.Y. Ye, X.R. Duan, *Fusion Eng. Des.* **139** (2019) 104.

[16] G. Zhuang, W. Liu, C. Yu, T. Lai, K. Zhai, C. Wang, Y. Wen, C. Wang, *Fusion Eng. Des.* **34** (1997) 411.

[17] M. Born and E. Wolf, *Principles of optics*, Pergamon Press (1980).

[18] C.V. Raman and N.S.N. Nath, *Proc. Ind. Acad. Sci. A* **2** (1935) 406, 413.

[19] S. Coda, Ph.D. Thesis, Massachusetts Institute of Technology (1997).

[20] H. Weisen, *Rev. Sci. Instrum.* **59** (1988) 1544.

[21] R. Nazikian and B. Grek, *Rev. Sci. Instrum.* **61** (1990) 2899.

[22] A. Marinoni, S. Coda, R. Chavan, G. Pochon, *Rev. Sci. Instrum.* **77** (2006) 10E929.

[23] A. Iantchenko, S. Coda, S. Brunner, G. Merlo, J. Ball, F. Margairaz, *Plasma Phys. Control. Fusion* **65** (2023) 025005.

[24] C.A. de Meijere, S. Coda, Z. Huang, L. Vermare, T. Vernay, V. Vuille, S. Brunner, J. Dominski, P. Hennequin, A. Krämer-Flecken, G. Merlo, L. Porte, L. Villard, *Plasma Phys. Control. Fusion* **56** (2014) 072001.

[25] Z. Huang, S. Coda, G. Merlo, S. Brunner, L. Villard, B. Labit, C. Theiler, *Plasma Phys. Control. Fusion* **60** (2018) 034007.

[26] Z. Huang, S. Coda, the TCV Team, *Plasma Phys. Control. Fusion* **61** (2019) 014021.

[27] S. Coda, A. Iantchenko, S. Brunner, M. Toussaint, K. Tanaka, *Nucl. Fusion* **61** (2021) 106022.